NASA TECHNICAL MEMORANDUM

NASA TM X-1821

NASA TM X-1821

ANALYSIS OF DYNAMIC JETTISON HINGE FORCES FOR CENTAUR NOSE FAIRING

by Hsin Ming Tang
Lewis Research Center
Cleveland, Ohio

NATIONAL AERONAUTICS AND SPACE ADMINISTRATION • WASHINGTON, D. C. • JULY 1969

NASA TM X-1821

ANALYSIS OF DYNAMIC JETTISON HINGE FORCES FOR CENTAUR NOSE FAIRING

By Hsin Ming Tang

Lewis Research Center
Cleveland, Ohio

NATIONAL AERONAUTICS AND SPACE ADMINISTRATION

For sale by the Clearinghouse for Federal Scientific and Technical Information
Springfield, Virginia 22151 – CFSTI price $3.00

ABSTRACT

Dynamic loads on nose fairing hinges are determined by a combination of tests and analyses. Transfer-function techniques are used. Hinge-force evaluations are determined according to normal mode theory for three-directional motion making use of data from tests of a fairing in a free-free end condition. A parametric study is presented of the hinge forces due to rigid body motion alone and combined motions of the rigid body and elastic modes.

ANALYSIS OF DYNAMIC JETTISON HINGE FORCES FOR CENTAUR NOSE FAIRING

by Hsin Ming Tang

Lewis Research Center

SUMMARY

An investigation of dynamic loads on the Centaur nose fairing hinges, occurring when the fairing is jettisoned, has been accomplished by tests and analysis. The methods of analysis used in this report is to employ transfer function concepts. The transfer function method is recommended for the determination of hinge loads, because the calculation is relatively simple and readily predicts the significance of the variation of each parameter to the dynamic loads. These analyses are based on normal mode theory for three-directional motion where data from tests of the nose fairing supported in a free-free end condition were used to determine the nose fairing dynamic characteristics. The results of the investigation presented in this report consist of parametric studies of the following five cases: (1) rigid-body responses in two directions, longitudinal and radial, with an elastic hinge; (2) rigid-body responses in radial direction at an infinitely stiff hinge joint; (3) rigid-body responses in radial direction at an elastic hinge joint; (4) superposition of rigid body and one modal response in radial direction at an elastic hinge joint; and (5) superposition of rigid body and two modal responses in radial direction at an elastic hinge joint. It was found from these studies that the hinge loads obtained from the rigid-body responses in two directions with an elastic hinge are adequate for design purposes.

INTRODUCTION

A test and analysis to determine dynamic loads on the Centaur nose fairing hinges, when the fairing is jettisoned, was performed in support of the sixth development flight of the Atlas-Centaur vehicle. The hinges are attached to the Centaur hydrogen tank at the junction of the forward end closure and cylinder (fig. 1). The hinges are relatively small, thus concentrating the loads and giving rise to the possibility of localized high stress.

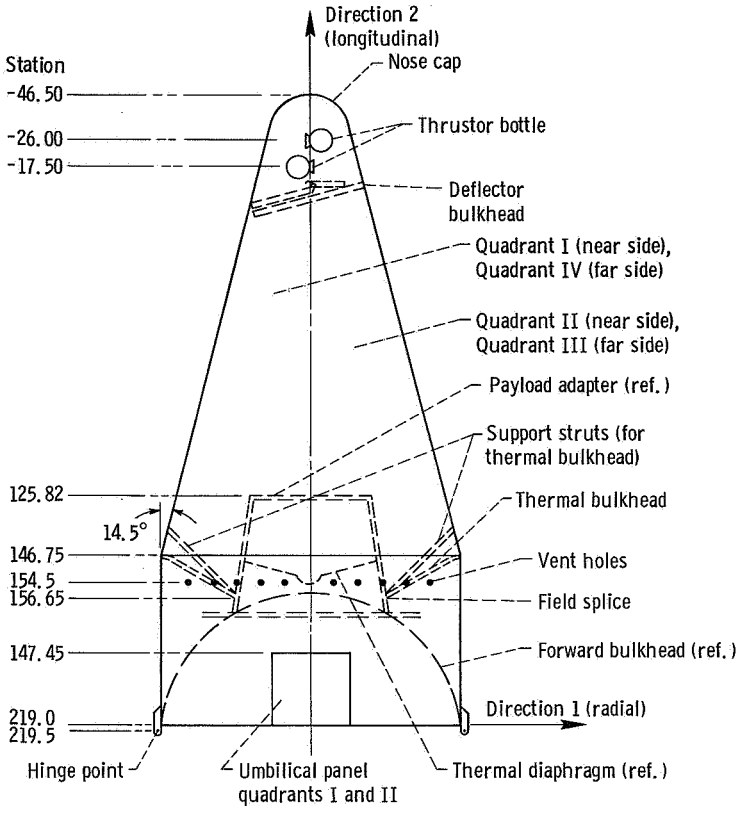

Figure 1. - Flight configuration of nose fairing.

The primary function of the fairing is to protect the spacecraft during ascent through the atmosphere. Separation of the fairing from the launch vehicle takes place after this function is accomplished. At the proper staging time, a command signal issued by the Atlas autopilot programmer initiates the separation and jettison procedure.

Nose fairing separation is accomplished by a shaped charge separation system which severs the structural joint between the nose fairing and the vehicle structure. The high frequency shock caused by an explosive shaped charge is usually associated with very small motions or strains and, in general, does not cause failure of the component parts of the vehicle. Thus, it will not be considered herein. Jettison forces which serve to rotate each fairing half about the hinge point are supplied by a high-pressure thrustor bottle filled with gaseous nitrogen.

The evaluation of the potentially large dynamic radial loads requires that the dynamic properties of the half nose fairing, such as natural frequencies, mode shapes, and structural damping, be well defined. For the nose fairing considered, the properties were determined by test of an actual nose fairing half (right half, quadrants II and III, as shown in fig. 1), which is shown in figure 2. Natural frequency resonances of the fairing half were located by a fast frequency sweep at constant g level. Subsequently, 10 successive

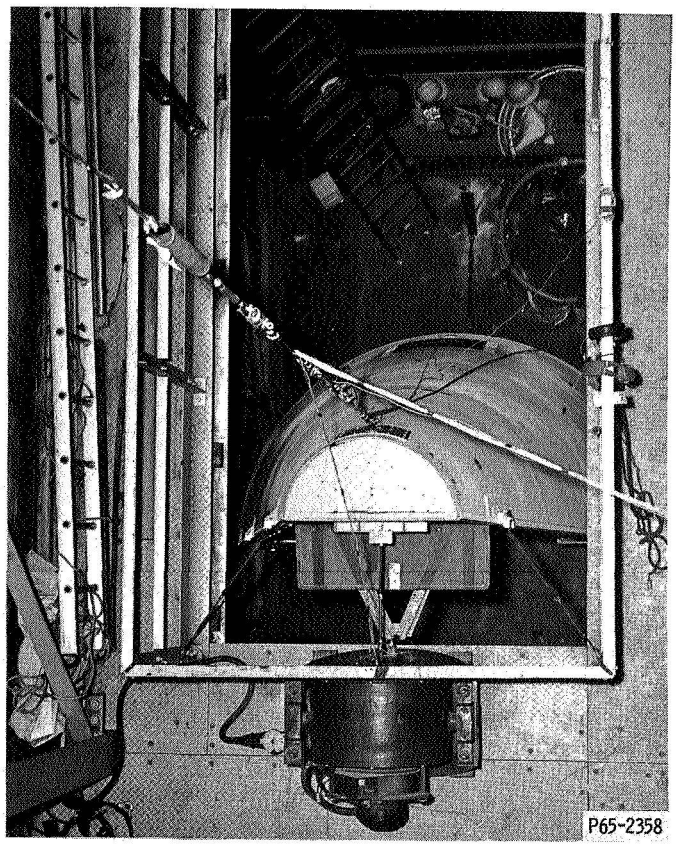

Figure 2. - Test configuration of nose fairing.

runs with small frequency increments in the vicinity of each resonant frequency were conducted in order to determine each resonant frequency more accurately. The structural damping for each mode was determined by logarithmic decay method. For each mode the amplitude ratios, mode shape, are normalized in terms of the reading of the accelerometer at location 12 m_{12} (see fig. 3).

The main objective of this report is to use the nose fairing dynamic properties from the test and a transfer function analysis to determine the hinge jettison radial loads of the fairing half. The analyses used herein are based on normal mode theory for three-directional motion to describe the fundamental dynamic characteristics of the nose fairing half. The transfer function method has the following advantages: (1) it simplifies the calculation and (2) it is easier to predict the results for variations of each parameter.

The hinge-force calculations presented herein consist of parametric studies of the following five cases: (1) rigid-body response in two directions, longitudinal and radial, with an elastic hinge, (2) rigid-body responses in the radial direction at an infinitely stiff hinge joint; (3) rigid-body responses in the radial direction at an elastic hinge joint; (4) superposition of rigid body and one modal response in the radial direction at an elas-

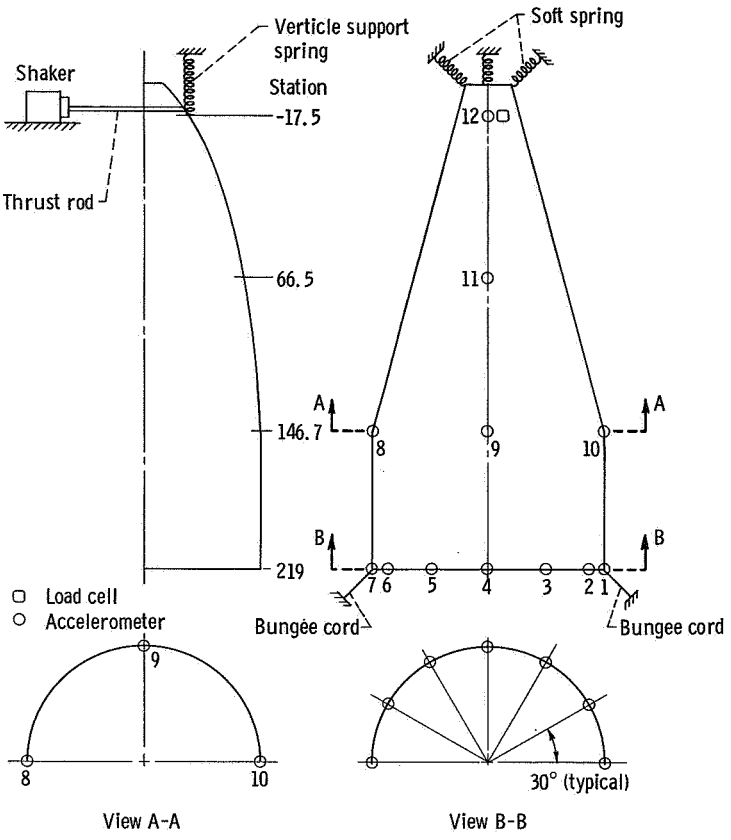

Figure 3. - Test setup and location of instrumentation.

tic hinge joint; and (5) superposition of rigid body and two modal responses in the radial direction at an elastic hinge.

METHOD OF ANALYSIS

The formulation of the problem via normal mode theory follows closely that of reference 1. The nose fairing is considered as an undamped linear elastic structure represented as lumped into n concentrated mass points each being capable of motion in two directions (planar motion). The relative displacement between m_j and the base (launch vehicle or test stand) in direction r is

$$X_j^r(t) = \sum_{a=1}^{2n} \overline{X}_{j,a}^r \, q_a(t) \tag{1}$$

where

$\bar{X}^r_{j,a}$ a^{th} modal deflection of m_j in direction r

$q_a(t)$ time function for displacement (normal coordinate, mode a)

(All symbols are defined in appendix A.) Also, from reference 1, we get

$$\ddot{q}_a(t) + (\omega_a)^2 q_a(t) = \frac{1}{M_a} \sum_{K=1}^{n} \sum_{S=1}^{2} \bar{X}^s_{Ka} \left(F^s_K + m_K g^s - m_K \ddot{Z}^s \right) \tag{2}$$

where

ω_a circular natural frequency, mode a

M_a modal mass, mode a, where

$$M_a = \sum_{j=1}^{n} \sum_{r=1}^{2} m_j \left(\bar{X}^r_{j,a} \right)^2$$

and

$$\sum_{j=1}^{n} \sum_{r=1}^{n} m_j \bar{X}^r_{j,a} \bar{X}^r_{j,b} = 0 \qquad a \neq b$$

F^s_K external force on m_K, direction s

m_j j^{th} concentrated mass

g^s acceleration due to gravity, direction s

$\ddot{Z}^s$ acceleration of base vehicle, direction s

Equations (1) and (2) form the starting point for the analyses of this report.

When the nose fairing is jettisoned, the nitrogen thrustor bottle force F^1_{12} (applied at m_{12}, direction 1) is the only true external force. However, as the normal mode shapes $\bar{X}^r_{j,a}$ in equations (1) and (2) are for free-free end conditions, the hinge forces are also to be considered as external forces F^r_4 (applied at m_4, directions 1 and 2).

Equations (2) can be expressed as

$$[\ddot{q}_a(t) + (\omega_a)^2 q_a(t)]\ M_a = \bar{X}^1_{12,a} F^1_{12} + \bar{X}^1_{4,a} F^1_4 + \bar{X}^2_{4,a} F^2_4 + \sum_{K=1}^{n} \sum_{s=1}^{2} \bar{X}^s_{K,a} m_K \left| g^s - \ddot{Z}^s \right| \quad (3)$$

where

F^1_{12} nitrogen thrustor bottle force, direction 1 (radial)

F^1_4 hinge force, direction 1 (radial)

F^2_4 hinge force, direction 2 (longitudinal)

Since a transfer function is desired, the Laplace transform (eq. (3)) with zero initial conditions is used to obtain

$$q_a(s) = \frac{\bar{X}^1_{12,a} F^1_{12} + \bar{X}^1_{4,a} F^1_4 + \bar{X}^2_{4,a} F^2_4 + \sum_{K=1}^{n} \sum_{s=1}^{2} \bar{X}^s_{K,a} m_K \left| g^s - \ddot{Z}^s \right|}{M_a[(s)^2 + (\omega_a)^2]} \quad (4)$$

The hinge spring forces are defined by

$$\left.\begin{aligned} F^1_4 &= -K_1 X^1_4 = -K_1 \sum_{a=1}^{2n} \bar{X}^1_{4,a} q_a \\ F^2_4 &= -K_2 X^2_4 = -K_2 \sum_{a=1}^{2n} \bar{X}^2_{4,a} q_a \end{aligned}\right\} \quad (5)$$

Using equations (4) and (5) the transfer functions for the responses of the hinge forces to the nitrogen thrustor bottle forces, gravity, and base motion are as follows:

$$F_4^1 = \frac{-K_1 \sum_{a=1}^{2n} \frac{\overline{X}_{4,a}^1 \left[\overline{X}_{12,a}^1 F_{12}^1 + \sum_{K=1}^{n} \sum_{s=1}^{2} \overline{X}_{K,a}^s m_K \left| g^s - \ddot{Z}^s \right| + \overline{X}_{4,a}^2 F_4^2 \right]}{M_a \left[(s)^2 + (\omega_a)^2 \right]}}{1 + K_1 \sum_{a=1}^{2n} \frac{\left[\overline{X}_{4,a}^1 \right]^2}{M_a \left[(s)^2 + (\omega_a)^2 \right]}} \tag{6a}$$

$$F_4^2 = \frac{-K_2 \sum_{a=1}^{2n} \frac{\overline{X}_{4,a}^2 \left[\overline{X}_{12,a}^1 F_{12}^1 + \sum_{K=1}^{n} \sum_{s=1}^{2} \overline{X}_{K,a}^s m_K \left| g^s - \ddot{Z}^s \right| + \overline{X}_{4,a}^1 F_4^1 \right]}{M_a \left[(s)^2 + (\omega_a)^2 \right]}}{1 + K_2 \sum_{a=1}^{2n} \frac{\left[\overline{X}_{4,a}^2 \right]^2}{M_a \left[(s)^2 + (\omega_a)^2 \right]}} \tag{6b}$$

Equations (6) are sufficient for the calculation of hinge forces. They are coupled, as F_4^1 responds to F_4^2, and vice versa. Although explicit solutions for each hinge force could easily be obtained, equations (6) are used herein for the responses.

It is useful, at this point, to insert into equations (6a) and (6b) the known and assumed characteristics of the free-free modes. Figure 4 defines a coordinate system and several parameters of interest for the nose fairing half. Table I contains the general information of the three free-free rigid-body modes and two free-free elastic modes.

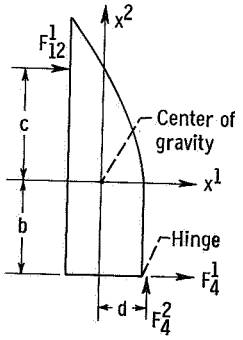

Figure 4. - Free-body diagram of nose fairing half.

TABLE I. - RIGID AND ELASTIC BODY MODES

Mode	Type	Natural (resonant) frequency, rad/sec	Mode shape	Modal mass, kg (a)
1	Rigid body translation direction 1	$\omega_1 = 0$	$\overline{X}^1_{j,1} = C_1$ $\overline{X}^2_{j,1} = 0$	$M_1 = (C_1)^2 M$
2	Rigid body translation direction 2	$\omega_2 = 0$	$\overline{X}^1_{j,2} = 0$ $\overline{X}^2_{j,2} = C_2$	$M_2 = (C_2)^2 M$
3	Rigid body rotation about center of gravity	$\omega_3 = 0$	$\overline{X}^1_{j,3} = C_3 x^2_j$ $\overline{X}^2_{j,3} = -C_3 x^1_j$	$M_3 = (C_3)^2 M(\rho)^2$
4	First elastic mode direction 1	$\omega_4 = 119.695$	$\overline{X}^1_{j,4}, \overline{X}^2_{j,4} = 0$	$M_4 = 5224$
5	Second elastic mode direction 2	$\omega_5 = 202.696$	$\overline{X}^1_{j,5}, \overline{X}^2_{j,5} = 0$	$M_5 = 4830$

[a]Total mass of half fairing $= M = \sum_{j=1}^{n} m_j$ and $M(\rho)^2 = I_{CG} = \sum_{j=1}^{n} m_j \left[\left(x^1_j \right)^2 + \left(x^2_j \right)^2 \right]$;

where x^1_j is the distance between m_j and center gravity of half fairing (direction 1) and x^2_j is the distance between m_j and center gravity of half fairing (direction 2).

Inserting the expressions from table I into equations (6) gives

$$F_4^1 = \frac{\left[\frac{bc}{(\rho)^2} - 1\right] F_{12}^1 - \frac{bd}{(\rho)^2} F_4^2 - \sum_{a=4}^{5} \frac{\bar{X}_{4,a}^1 \bar{X}_{12,a}^1 M(S)^2 F_{12}^1}{M_a\left[(S)^2 + (\omega_a)^2\right]}}{1 + \left(\frac{b}{\rho}\right)^2 + \frac{M}{K_1}(S)^2 + \sum_{a=4}^{5} \left[\bar{X}_{4,a}^1\right]^2 \frac{M(S)^2}{M_a\left[(S)^2 + (\omega_a)^2\right]}} \tag{7a}$$

$$F_4^2 = \frac{\frac{dc}{(\rho)^2} F_{12}^1 - \frac{bd}{(\rho)^2} F_4^1 + \left|\ddot{Z}^2 - g^2\right| M}{1 + \left(\frac{d}{\rho}\right)^2 + \frac{M}{K_2}(S)^2} \tag{7b}$$

where we assume $g^1 - \ddot{Z}^1 = 0$. The equations are presented in matrix form in appendix B.

DESCRIPTION OF TEST PROCEDURE

The test data to be used in this report were obtained during preflight evaluation tests of the Centaur nose fairing. Details of the method and procedure are included since the data have not been published elsewhere.

Test Setup

The dynamic test of the nose fairing half was conducted at the E-site test stand of Plum Brook Station of Lewis Research Center. The test specimen consisted of the right half (quadrants II and III, as shown in fig. 1) of the nose fairing for the sixth development flight version of the Atlas-Centaur launch vehicle. The fairing half was suspended in the vertical direction (as shown in figs. 2 and 3) to simulate free-free boundary conditions for the lateral bending modes. Two soft springs were provided at the upper corners and two bungee cords at the bottom to prevent the fairing half from twisting. Figure 2 also shows the location of the shaker with the centerline of the thrust rod situated colinear with the centerline of the nitrogen thrust bottle (vehicle station -17.50, fig. 1). Figure 3 shows the location of 12 accelerometers and one load cell. The responses were

measured in the radial direction only. Since the responses in the tangential direction are shown in unpublished test results (obtained by General Dynamics/Convair Div. under NASA contract NAS3-7417) to be negligibly small, the responses in the tangential direction are neglected.

Test Procedure

An approximate value of each resonant frequency was determined by a fast frequency sweep for a constant load level. Subsequently, 10 successive runs with small frequency increments in the vicinity of each resonant frequency were conducted in order to determine each resonant frequency more accurately.

The structural damping for each mode was determined by the logarithmic decay method. The data for these calculations were obtained by uncoupling the shaker from the test specimen when a natural frequency was excited.

DATA ANALYSIS

Only one shaker was used to excite the nose fairing specimen. For the higher modes, the data indicated that the lateral modes are coupled with shell modes. Thus, only the first two modes are used in the present analysis. For the higher modes a test utilizing several shakers would be necessary for a better evaluation. The test data were analyzed for natural frequencies, structural damping, and generalized mass. The method of analysis is discussed in the following paragraphs and the results are presented in table II.

Natural Frequencies and Structural Damping

Each natural frequency is determined from the peak point of a plot of the previously mentioned 10 successive readings at accelerometer location 12 m_{12} against frequency. The structural damping at each accelerometer location m_j for each mode is obtained by means of the logarithmic decay method as expressed in reference 2.

Mode Shapes

Phase angles and amplitude ratios of each mode were obtained by processing FM tape recordings into an analog computer mechanization of a harmonic analyzer. At each

TABLE II. - TEST DATA:

DYNAMIC PROPERTIES OF NOSE FAIRING HALF

First elastic mode[a]		Second elastic mode[b]	
Accelerometer, m_j	Damping ratio, ζ_4	Accelerometer, m_j	Damping ratio, ζ_5
1	0.007648	1	0.009753
2	.007054	2	.015960
3	.010362	3	.013109
4	.010506	4	.011116
5	.007357	5	.011077
6	.006045	6	.009315
7	.007234	7	.013580
8	.007733	8	.007322
9	.007175	9	.010830
10	.007890	10	.007264
11	.007404	11	.010091
12	.007052	12	.010830

[a]Frequency, f_4, 19.05 Hz; total mass of half fairing, M_4, 358 slugs (5224.6162 kg); first elastic modal deflection of m_4 (hinge) in direction 1 (radial), $\bar{X}^1_{4,4}$, 0.375; first elastic modal deflection of m_{12} in direction 1 (radial), $\bar{X}^1_{12,5}$, 1.

[b]Frequency, f_5, 32.26 Hz; total mass of half fairing, M_5, 331 slugs (4830.5890 kg); second elastic modal deflection of m_4 (hinge) in direction 1 (radial), $\bar{X}^1_{4,5}$, 0.416; second elastic modal deflection of m_{12} in direction 1 (radial), 1.

resonant frequency the amplitude ratios determined the mode shape and were normalized in terms of the readings of the accelerometer location 12 m_{12} (fig. 3).

The first two mode shapes along the fairing centerline, obtained from the test, are presented in figures 5. In these figures the cross-sectional view at stations 146 and 219 indicate the shell mode excitation.

Model Mass

The following discussion pertains to the evaluation of the model mass for each of two elastic modes (direction 1) by making use of single degree of freedom analogy together with the test results. As mentioned previously, the only input to the structure is at accelerometer location 12 m_{12}, and the responses of the structure are normalized at the same location.

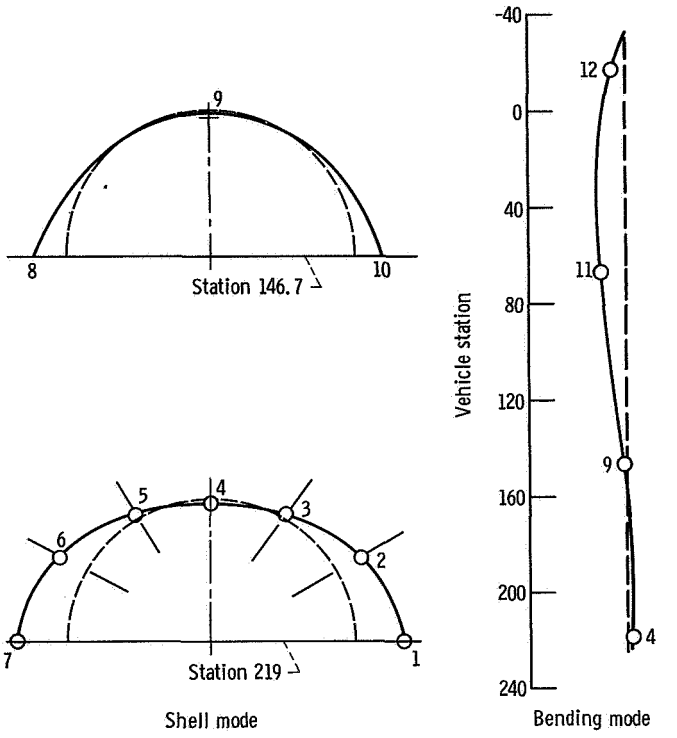

(a) First mode; natural frequency, 19.05 hertz.

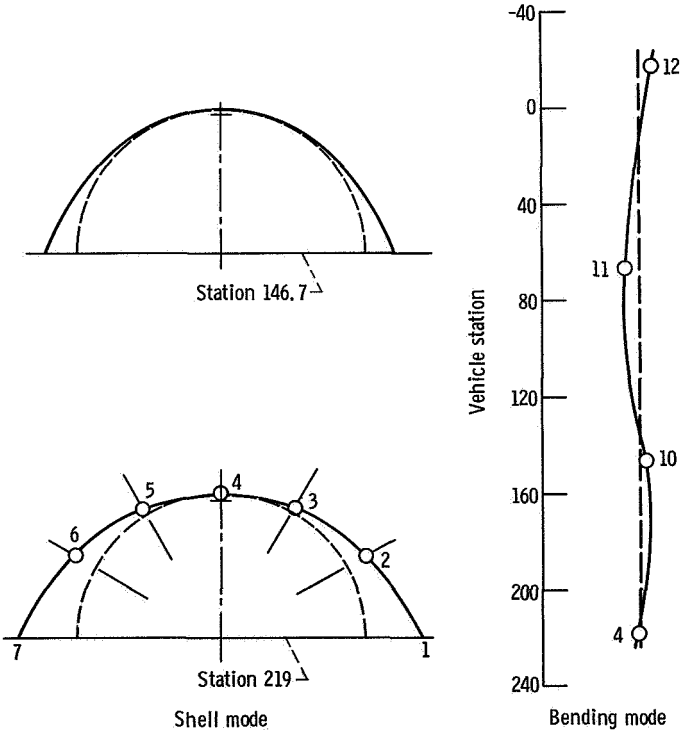

(b) Second mode; natural frequency, 32.26 hertz.

Figure 5. - Mode shapes.

From equations (1) and (4) and including modal damping, the general response in acceleration for the free-free system is given by

$$\ddot{X}_j^1 = \sum_{a=4}^{5} \bar{X}_{j,a}^1 \frac{\bar{X}_{12,a}^1 (S)^2}{M_a\left[(S)^2 + (\omega_a)^2 + 2\zeta_a \omega_a S\right]} \cdot F_{12}^1 \tag{8}$$

where $\ddot{Z} = F_4 = 0$ and gravity force can be omitted for the elastic modes (ref. 2). For an oscillatory excitation force at location 12 of frequency $\omega_b (S = i\omega_b)$ equation (8) becomes

$$\ddot{X}_j^1 = \sum_{a=4}^{5} \bar{X}_{j,a}^1 \frac{-\bar{X}_{12,a}^1 (\omega_b)^2 F_{12}^1}{M_a\left[i(2\zeta_a \omega_a \omega_b) + (\omega_a)^2 - (\omega_b)^2\right]} \tag{9}$$

The term in the sum with $a = b$ will dominate the right side of the above equation and we will have

$$\bar{X}_j^1 = \frac{\left(\bar{X}_{j,b}^1 \bar{X}_{12,b}^1 F_{12}^1\right) i}{M_b 2\zeta_b} \tag{10}$$

Using the accelerometer at location 12 m_1, to determine M_b gives

$$M_b = \frac{\left[\bar{X}_{12,b}^1\right]^2}{2\zeta_b} \left| \frac{i\left(F_{12}^1\right)}{\bar{X}_{12}^1} \right| \tag{11}$$

HINGE FORCE EVALUATION

Jettison Force

During nose fairing jettison, the total jettison forces occurring on each fairing half are due to the combination of three loadings: (1) thrust from the bottle, (2) gas impinge-

ment from the opposite thrustor bottle, and (3) static pressure within the nose fairing upper cavity. Figures 6 to 9 show the time variations of these forces, respectively. The data for these figures are from Convair Division of General Dynamics Company sources (under NASA contract NAS3-8701) and are based on an initial bottle pressure of 2450 psi (1.68922×10^6 N/m^2).

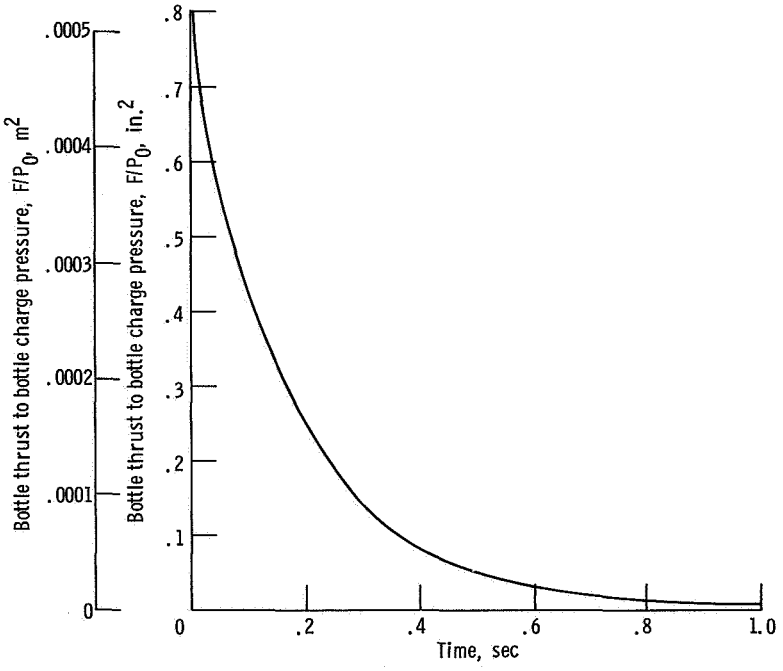

Figure 6. - Thrustor bottle variation of bottle thrust characteristics with time; pressure, 1.68922×10^6 N/m^2

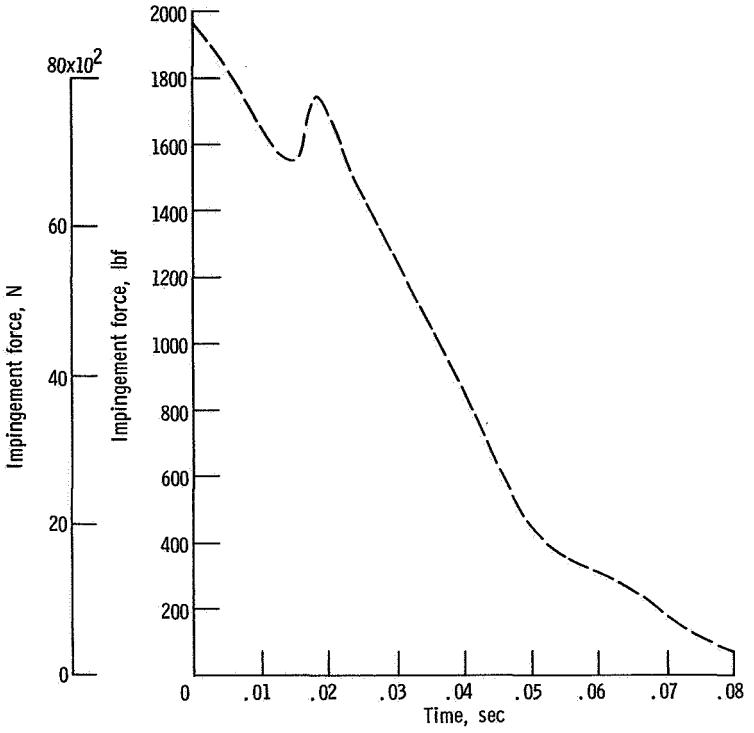

Figure 7. - Nose fairing variation of impingement forces with time.

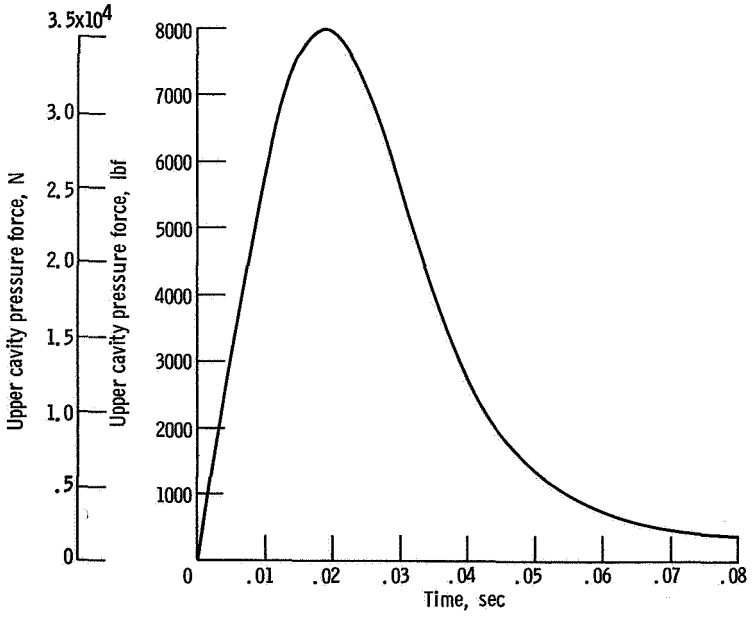

Figure 8. - Nose fairing variation of upper cavity pressure force with time.

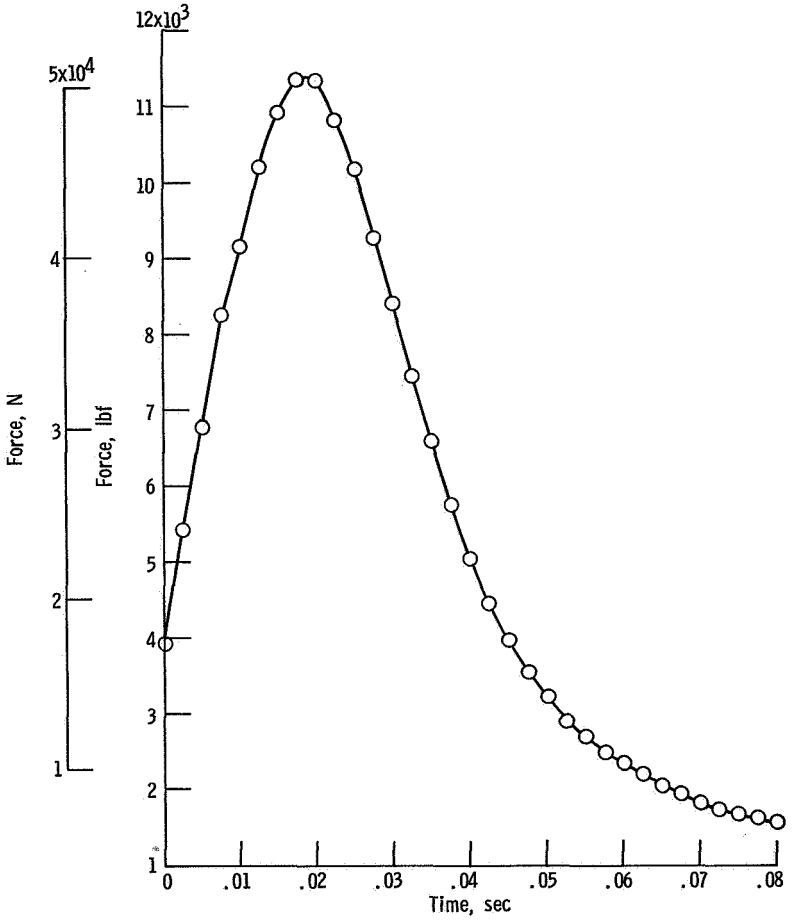

Figure 9. - Resultant of jettison forces.

Hinge Forces

The results presented herein consist of parametric studies of the following five cases: (1) rigid-body responses in two directions, longitudinal and radial, with an elastic hinge; (2) rigid-body responses in the radial direction at an infinitely stiff hinge joint; (3) rigid-body responses in the radial direction at an elastic hinge joint; (4) superposition of rigid body and one modal response in the radial direction at an elastic hinge joint; and (5) superposition of rigid body and two modal responses in the radial direction at an elastic hinge joint.

Figures 10 and 11 give the transient responses for the hinge forces under various conditions and assumptions. Figure 12 shows frequency responses for 2 special cases.

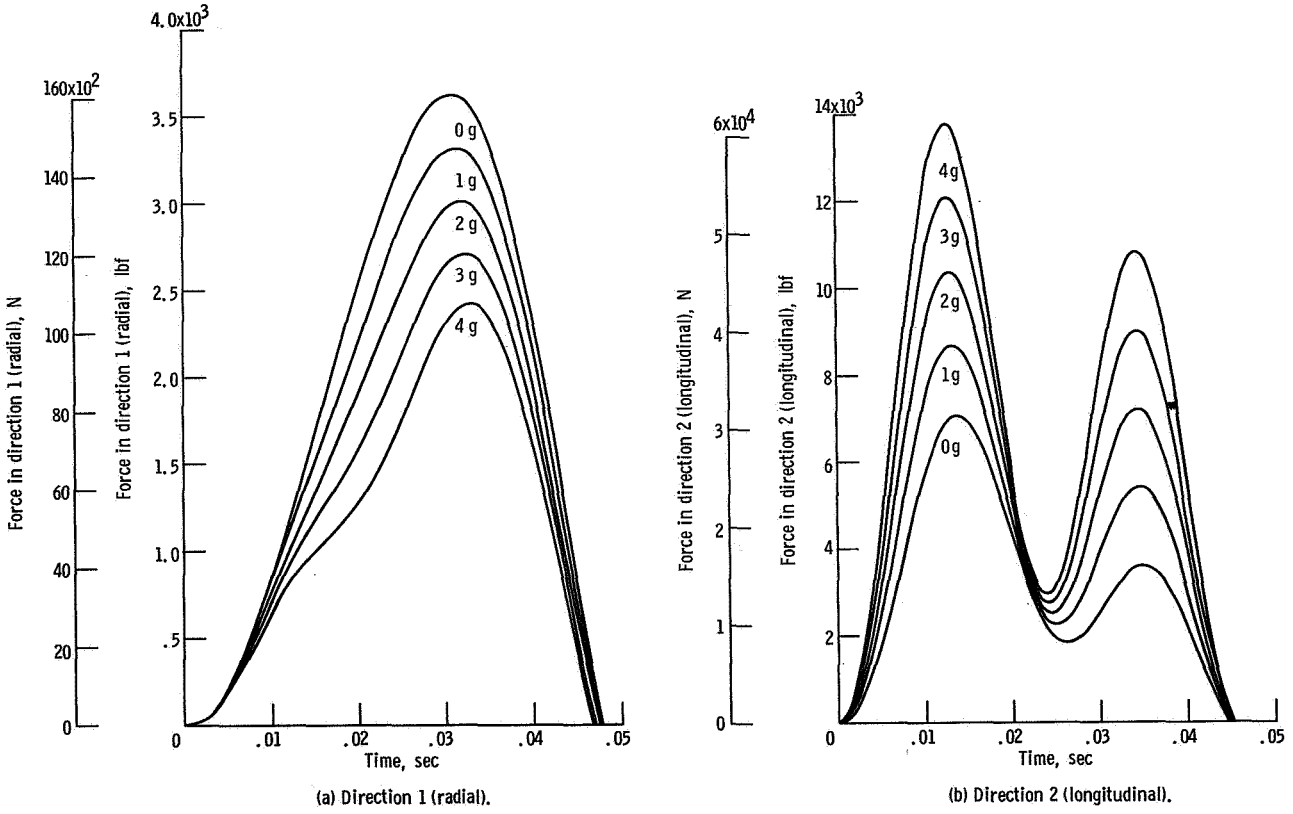

(a) Direction 1 (radial).

(b) Direction 2 (longitudinal).

Figure 10. - Rigid body response for hinge force.

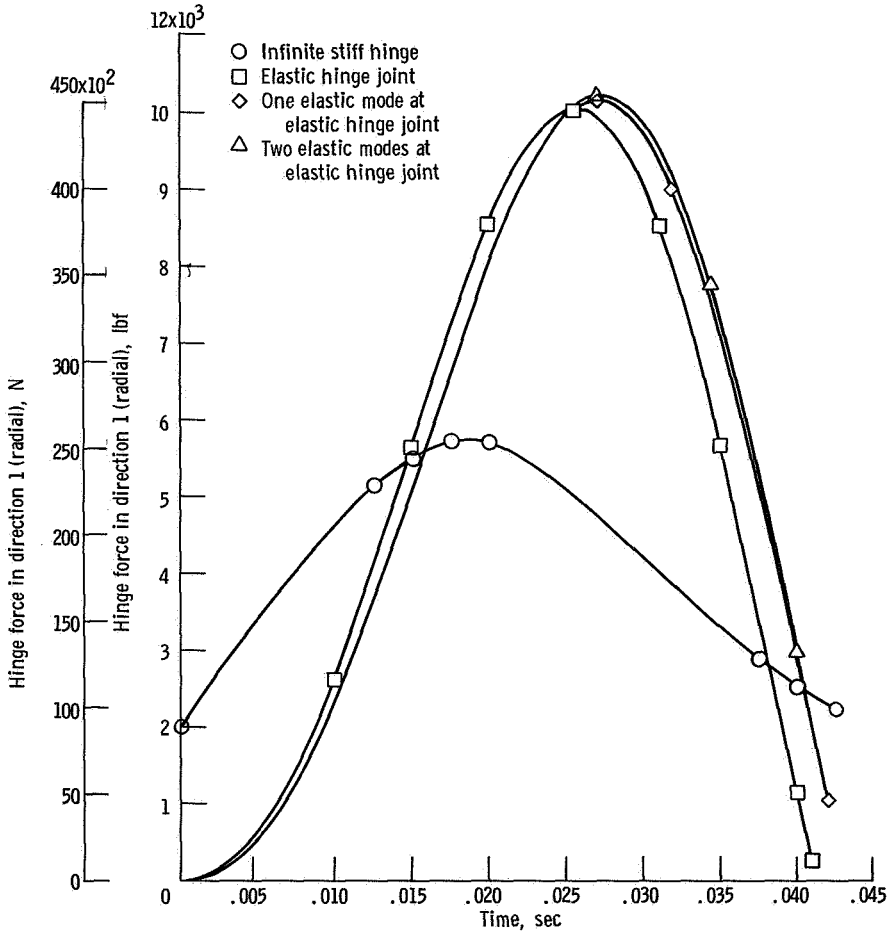

Figure 11. - Hinge force variation with time for hinge-free beam.

DISCUSSION

The transient hinge loads (fig. 10) were obtained by solving the differential equations represented by the transfer functions of equation (7), ignoring the elastic modes and using values of pertinent parameters given in table III. The inputs were the total bottle force (fig. 9) and various levels of $(\ddot{Z}^2 - g^2)$ included as a step input. This assumes that the nose fairing half is entirely supported by the hinge joint for time greater than zero.

TABLE III. - NOSE FAIRING PARAMETERS

Hinge spring constant (direction 1), K_1, lbf/in.; N/m	17 800; 3.11726×10^6
Hinge spring constant (direction 2), K_2, lbf/in.; N/m	171 000; 2.99467×10^7
Total mass of half fairing, M, slugs; kg	30.3916; 443.532
Radius of gyration, ρ, in.; m	93.766; 2.3817
Distance between center of gravity of nose fairing half and hinge point (direction 2), b, in.; m	94; 2.3876
Distance between center of gravity of nose fairing half and point of applied jettison force, c, in.; m	142.5; 3.6195
Distance between center of gravity of nose fairing half and hinge point (direction 1), d, in.; m	32.57; 0.8273

As the vehicle thrust level increased from 0 to 4 g, the peak radial hinge load decreased from 3625 to 2425 pounds (16 125 to 10 787 N), and the shape of the transient curve remained unchanged. The effects of vehicle thrust level on the longitudinal hinge load is much greater. As thrust level increased from 0 to 4 g, the peak longitudinal hinge load increased from 7050 to 13 800 pounds (31 360 to 61 385 N).

The transient hinge loads (fig. 11) were obtained from equation (7a) for $d = 0$, that is, for no offset in the center of gravity location or an equivalent beam. It is apparent from the results on figure 11 that ignoring the hinge support elasticity would give a low peak hinge load and nonoscillatory response. It is sufficient to consider a rigid-body fairing with an elastic hinge support to obtain correct peak hinge loads and even total response. Including the first elastic mode of fairing delays the response slightly but does not affect peak load. Including the second elastic mode has almost no effect. Comparing figures 10 and 11 shows that the center of gravity offset d considerably reduced the radial hinge loads.

Test results as presented in table II and the previous discussion show that the elastic mode terms in equation (7a) are small; hence, they can be ignored when using both equations of (7a) and (7b). Figure 10(a) shows that the calculated hinge peak load in the radial direction is 3300 pounds (14 679 N) at the 1-g level. This value is in good agreement with unpublished test results of 2500 to 3750 pounds (11 121 to 16 681 N)

(obtained by Humphery and Eastwood of Lewis). Thus, the results of figure 10 are valid and represent the best estimate of the hinge loads. One should expect some variation between the test and analytical results due to redundant load path, clearance gaps in the hinge and other constraints, which are not included in the analysis but do affect the test results.

Rigid Body Fairing, Rigid Longitudinal Hinge Spring

This case is relatively valid and simple to express. From equations (7a) and (7b) with $K_2 \to \infty$ and ignoring the elastic modes, we get

$$F_4^1 = \frac{\left[\frac{bc}{(\rho)^2} - 1 - \frac{(d)^2}{(\rho)^2}\right] F_{12}^1 - \frac{bd}{(\rho)^2} M\left|\ddot{Z}^2 - g^2\right|}{1 + \frac{(b)^2 + (d)^2}{(\rho)^2} + \left[1 + \frac{(d)^2}{(\rho)^2}\right] \frac{M(S)^2}{K_1}} \tag{12}$$

It is readily seen why including d decreased the radial hinge load.

If the coefficient of F_{12}^1 is zero, only effects of vehicle thrust level produces radial hinge loads. This condition (bottle force at center of percussion) is given by

$$c = \frac{(\rho)^2 + (d)^2}{b} \tag{13}$$

It would be expected that the bottle force at the center of percussion would considerably reduce the radial hinge loads. There would still be small additional loads due to longitudinal hinge spring and elastic modes effects.

Frequency Response

The combined effects of the fairing bearing on an elastic hinge joint and one or two elastic modes of the free-free fairing are considered. Equations (7) are used for the case of $d = 0$. Substituting the dynamic and physical properties of the fairing obtained

from tables II and III into equations (7) yields:

$$\frac{F^1_{4(S)}}{F^1_{12(S)}} = \frac{1.25543 + 0.03171\,\dfrac{(S)^2}{(S)^2 + (\omega_4)^2} - 0.03813\,\dfrac{(S)^2}{(S)^2 + (\omega_5)^2}}{2.48779 + 0.00014205\,(S)^2 + 0.01189\,\dfrac{(S)^2}{(S)^2 + (\omega_4)^2} + 0.01586\,\dfrac{(S)^2}{(S)^2 + (\omega_5)^2}} \tag{14}$$

The coefficients of the additional terms giving the contribution due to the fairing elastic modes are small relative to the constant terms. At infinite frequencies these terms take on these values; at very small frequencies, the contribution is still smaller. Only at the resonant frequencies of the fairing elastic modes would these terms have any appreciable effect. At $S = i\omega_4$,

$$\frac{F^1_4}{F^1_{12}} = \frac{0.03171}{0.01189} = 2.667 \tag{15}$$

At $S = i\omega_5$

$$\frac{F^1_4}{F^1_{12}} = \frac{-0.03813}{0.01586} = -2.4042 \tag{16}$$

This effect occurs over a narrow frequency band and apparently does not appreciably affect overall transient response.

The frequency responses shown in figure 12 reveal additional features of the effect of the elastic modes. Evidently, at the resonant frequency of approximately 19 hertz, the transfer function has also a zero (i.e., a dipole occurs at this frequency) so that the effect of this resonance is nil. The same is true to a lesser extent at the upper resonant frequency of approximately 32.3 hertz. So that, except for strong inputs of very narrow band around 32.3 hertz, we would expect the effects of elastic modes to be negligible for the nose fairing studied herein.

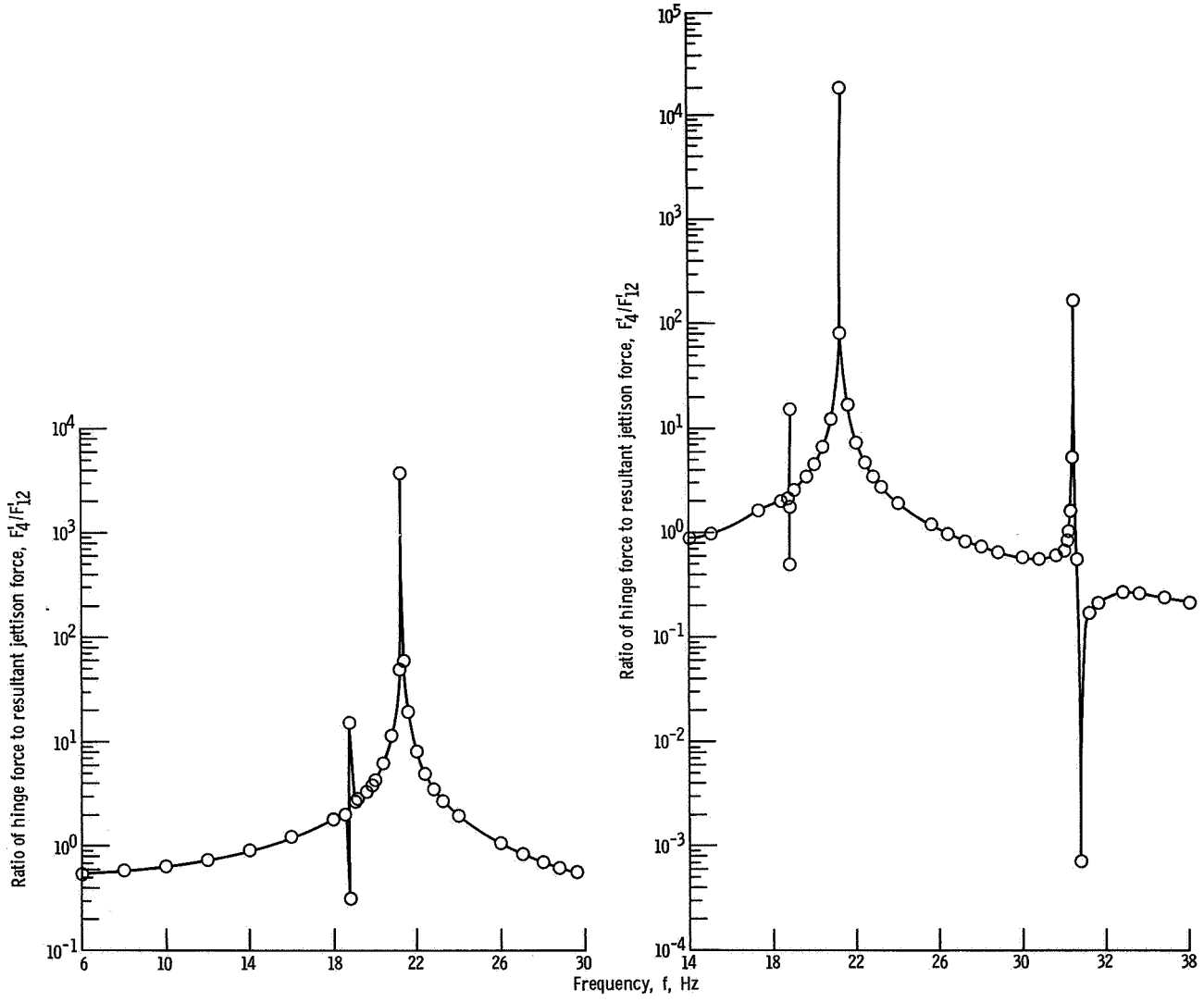

(a) Rigid body plus one elastic mode at elastic hinge.

(b) Rigid body plus two elastic modes at elastic hinge.

Figure 12. - Frequency spectrum for hinge-free beam.

CONCLUDING REMARKS

The transfer function method is recommended for use in the hinge load calculation. It has two definite advantages: (1) it simplifies the calculation, and (2) it is easier to predict the significance of variation of each parameter.

Results obtained from this investigation show that the hinge loads obtained from the rigid-body responses with an elastic hinge can be used for the design purposes since the elastic-body modal responses have negligible effects for the nose fairing considered.

Lewis Research Center,
National Aeronautics and Space Administration,
Cleveland, Ohio, March 6, 1969,
124-08-05-01-22.

APPENDIX A

SYMBOLS

b distance between center of gravity of nose fairing half and m_4 (hinge point), direction 2, in.; cm

C_1, C_2 constants

C_3 constant, $in.^{-1}$; cm^{-1}

c distance between center of gravity of nose fairing half and m_{12} (point of applied jettison force), direction 2, in.; cm

d distance between center of gravity of nose fairing and m_4 (hinge point), direction 1, in.; cm

F_K^s external force on m_K, direction s, N

f_a natural frequency, Hz

g^s acceleration due to gravity, direction s, ft/sec^2; cm/sec^2

I_{CG} moment of inertia about center of gravity of fairing half, $I_{CG} = M(\rho)^2$, $(lbm)(ft^2)$; $(kg)(m^2)$

K_1 hinge spring constant, direction 1, lbf/in.; N/m

K_2 hinge spring constant, direction 2, lbf/in.; N/m

M total mass of half fairing, lbm; kg

M_a modal mass, mode a, $M_a = \sum_{j=1}^{n} \sum_{r=1}^{2} m_j (\overline{X}_{j,a}^r)^2$

M_1 modal mass for rigid body translational mode, direction 1 ($M_1 = (C_1)^2 M$), lbm; kg

M_2 modal mass for rigid body translational mode, direction 2 ($M_2 = (C_2)^2 M$), lbm; kg

M_3 modal mass for rigid body rotational mode about center of gravity, $M_3 = (C_3)^2 M(\rho)^2$, lbm; kg

M_4 modal mass for first elastic mode, direction 1, lbm; kg

M_5 modal mass for second elastic mode, direction 1, kg

m_K K^{th} concentrated mass, lbm; kg

$q_a(t)$ time function for displacement (normal coordinate, mode a), in.; cm

$\ddot{q}_a(t)$ second derivation of q_a with respect to time

S Laplace operator

X_j^r relative displacement between m_j and base (vehicle), direction r, in.; cm

$\overline{X}_{j,a}^r$ a^{th} modal deflection of m_j in direction r

x_j^1 distance between m_j and center of gravity of half fairing, direction 1, in.; cm

x_j^2 distance between m_j and center of gravity of half fairing, direction 2, in.; cm

$\ddot{Z}^s$ acceleration of base (vehicle), direction S, ft/sec^2; m/sec^2

ζ_a damping ratio, mode a

ρ radius of gyration, in.; cm

ω_a circular natural frequency, mode a, rad/sec

Subscripts:

a, b normal modes

i, j, k mass points

Superscripts:

r, S direction r, S

T transpose of matrix

$(\omega_a)^2$ square of ω_a (to avoid confusion with direction superscript, quantities are placed inside brackets when raising to power)

1 radial direction

-1 inverse of matrix

2 longitudinal direction

APPENDIX B

MATRIX FORM OF HINGE LOAD EQUATIONS

In order to formulate the problem in convenient vector and matrix forms for ease of manipulation and analogous to one-dimensional structure dynamic problems, the following vectors and matrices are defined:

$$x = \begin{Bmatrix} x_j^1 \\ x_j^2 \end{Bmatrix} \begin{matrix} \}n \\ \}n \end{matrix} \qquad \bar{x} = \begin{Bmatrix} \bar{x}_{ja}^1 \\ \bar{x}_{ja}^2 \end{Bmatrix} \begin{matrix} \}n \\ \}n \end{matrix}$$

number of modes

$$F = \begin{Bmatrix} F_j^1 \\ F_j^2 \end{Bmatrix} \begin{matrix} \}n \\ \}n \end{matrix} \qquad m = \begin{bmatrix} m_1 & & & & & & 0 \\ & m_2 & & & & & \\ & & m_n & & & & \\ & & & m_1 & & & \\ & 0 & & & m_2 & & \\ & & & & & m_n & \end{bmatrix} \qquad g = \begin{Bmatrix} g^1 \\ g^1 \\ g^1 \\ g^2 \\ g^2 \\ g^2 \end{Bmatrix} \qquad z = \begin{Bmatrix} z^1 \\ z^1 \\ z^1 \\ z^2 \\ z^2 \\ z^2 \end{Bmatrix}$$

Then equations (1) and (2) become

$$x = \bar{x}q \tag{B1}$$

$$\ddot{q} + (\omega)^2 q = M^{-1}\bar{x}^T [F + m|g - \ddot{z}|] \tag{B2}$$

where

ω^2 diagonal $(\omega_1^2, \omega_2^2, \ldots)$

m $\bar{x}^T m \bar{x}$ = diagonal $(M_1, M_2, \ldots)$

The forces F can be separated into two parts, internal forces (hinge forces) and external forces (nitrogen thrustor bottle forces). Thus,

$$F = F_{hinge} + F_{ext}$$

and equation (B2) becomes

$$\ddot{q} + \omega^2 q = \overline{M}^1 \overline{x}^T (F_{hinge} + F_{ext} + m|g - \ddot{z}|) \tag{B3}$$

Taking the Laplace transform, with zero initial conditions, of equation (B3) and solving for q(s) gives

$$q(s) = [(s)^2 + (\omega)^2]^{-1} M^{-1} \overline{x}^T (F_{hinge} + F_{ext} + m|g - \ddot{z}|) \tag{B4}$$

The hinge spring forces are defined by

$$F_{hinge} = -Kx = -K\overline{x}q \tag{B5}$$

Using equations (B4) and (B5), the following equation relates the hinge force to the nitrogen thrustor bottle force F_{ext}, gravity, and base motion.

$$\left\{\delta + K\overline{x}[(s)^2 + (\omega)^2]^{-1} M^{-1} \overline{x}^T\right\} F_{hinge} = -Kx[(s)^2 + (\omega)^2]^{-1} M^{-1} \overline{x}^T F_{ext} + m|g - \ddot{z}| \tag{B6}$$

REFERENCES

1. Cunniff, P. F.; and O'Hara, G. J.: Normal Mode Theory for Three-Directional Motion. NRL-6170, U.S. Naval Research Lab., Jan. 5, 1965. (Available from DDC as AD-611573.)

2. Thomson, William T.: Vibration Theory and Applications. Prentice-Hall, Inc., 1965.

NASA-Langley, 1969 —— 32 E-4918

"The aeronautical and space activities of the United States shall be conducted so as to contribute . . . to the expansion of human knowledge of phenomena in the atmosphere and space. The Administration shall provide for the widest practicable and appropriate dissemination of information concerning its activities and the results thereof."

—NATIONAL AERONAUTICS AND SPACE ACT OF 1958

NASA SCIENTIFIC AND TECHNICAL PUBLICATIONS

TECHNICAL REPORTS: Scientific and technical information considered important, complete, and a lasting contribution to existing knowledge.

TECHNICAL NOTES: Information less broad in scope but nevertheless of importance as a contribution to existing knowledge.

TECHNICAL MEMORANDUMS: Information receiving limited distribution because of preliminary data, security classification, or other reasons.

CONTRACTOR REPORTS: Scientific and technical information generated under a NASA contract or grant and considered an important contribution to existing knowledge.

TECHNICAL TRANSLATIONS: Information published in a foreign language considered to merit NASA distribution in English.

SPECIAL PUBLICATIONS: Information derived from or of value to NASA activities. Publications include conference proceedings, monographs, data compilations, handbooks, sourcebooks, and special bibliographies.

TECHNOLOGY UTILIZATION PUBLICATIONS: Information on technology used by NASA that may be of particular interest in commercial and other non-aerospace applications. Publications include Tech Briefs, Technology Utilization Reports and Notes, and Technology Surveys.

Details on the availability of these publications may be obtained from:

SCIENTIFIC AND TECHNICAL INFORMATION DIVISION

NATIONAL AERONAUTICS AND SPACE ADMINISTRATION

Washington, D.C. 20546